Effects of Water and Cell Culture Media on the Physicochemical Properties of ZnMgO Nanoparticles and Their Toxicity toward Mammalian Cells

Jasmina Vidic, Francia Haque, Jean Michel Guigner, Aurore Vidy, Christophe Chevalier, Slavica Stankic

Langmuir

Article

Effects of water and cell culture media on the physicochemical properties of ZnMgO nanoparticles and their toxicity towards mammalian cells

Jasmina Vidic, Francia Haque, Jean-Michel Guigner, Aurore Vidy, Christophe Chevalier, and Slavica Stankic

Langmuir, **Just Accepted Manuscript** • DOI: 10.1021/la501479p • Publication Date (Web): 03 Sep 2014

Effects of water and cell culture media on the physicochemical properties of ZnMgO nanoparticles and their toxicity towards mammalian cells

Jasmina Vidic[1*], Francia Haque[2,3], Jean Michel Guigner[4,5], Aurore Vidy[1], Christophe Chevalier[1], Slavica Stankic[2,3*]

[1] Virologie et Immunologie Moléculaires, Institut de la Recherche Agronomique, UR 892, Bât. Biotechnologies, Jouy en Josas, France.

[2] CNRS, Institut des Nanosciences de Paris, UMR 7588, 4 place Jussieu, 75252 Paris Cedex05, France.

[3] UPMC – Université Paris 06, INSP, UMR 7588,4 place Jussieu, 75252 Paris Cedex05, France.

[4] IMPMC – Institut de Minéralogie et de Physique des Milieux Condensés, Université Pierre et Marie Curie, UMR7590, 4 place Jussieu, 75252 Paris Cedex05 France.

[5] CNRS, IMPMC-UMR7590, Paris, F-75005 France.

[*]Corresponding authors:

Jasmina Vidic, e-mail: jasmina.vidic@jouy.inra.fr ; tel : + 33134652623; fax : +33134652621

Slavica Stankic, e-mail: slavica.stankic@insp.jussieu.fr; tel: + 33144274650; fax: + 33144273982

Abstract

ZnMgO nanoparticles have shown potential for medical applications as an efficient antibacterial agent. In this work, we investigate the effect of water and two commonly used cell culture media on the physicochemical properties of ZnMgO nanoparticles in correlation with their cytotoxicity. In vacuum, ZnMgO nanopowder consists of MgO (nanocubes) and ZnO (nanotetrapods and nanorods) particles. Upon exposure to water or the Luria-Bertani solution, ZnO characteristic shapes were not observable while MgO nanocubes transformed into octahedral form. In addition, water caused morphological alternations in form of disordered and fragmented structures. This effect was directly reflected in UV/Vis absorption properties of ZnMgO implying that formation of new states within the band gap of ZnO and redistribution of specific sites on MgO surfaces occurs in presence of water. In mammalian culture cell medium, ZnMgO nanoparticles were shapeless, agglomerated and coated with surrounding proteins. Serum albumin was found to adsorb as a major but not the only protein. Adsorbed albumin mainly preserved its α-helix secondary structure. Finally, the cytotoxicity of ZnMgO was shown to strongly depend on the environment: in the presence of serum proteins ZnMgO nanopowder was found to be safe for mammalian cells while highly toxic in a serum-free medium or a medium containing only albumin. Our results demonstrate that nanostructured ZnMgO reaches living cells with modified morphology and surface structure when compared to as-synthetized particles kept in vacuum. In addition, its biocompatibility can be modulated by proteins from biological environment.

Introduction

Nanostructured metal oxides are being incorporated into almost all fields of technology: fabrication of microelectronic circuits, sensors, piezoelectric devices, fuel cells, coatings for the passivation of surfaces against corrosion, and as catalysts.[1, 2] This is due to their electronic structure which can exhibit a metallic, semiconducting or insulating character. Metal oxide nanoparticles are furthermore used to enhance the quality of cosmetic and food industry products, whereas medical purposes include their applications such as therapeutics, diagnostics, imaging or drug deliveries.[3, 4, 5] Metal oxides, such as ZnO, MgO, CuO or TiO_2, have a particular potential for the use in medicine due to their strong antimicrobial activity against a range of bacteria.[6, 7, 8, 9] Several mechanisms of antibacterial action have been proposed, such as mechanical damaging of bacterial membranes, cell penetration and binding to specific intracellular targets, and/or generation of reactive oxygen species.[7] These findings suggested that metal oxide nanoparticles may provide novel modes of action when compared to existing antibiotics and, so they can potentially be applied against strains of bacteria with gained antibiotics resistance. To date, however, their biocompatibility and the safety for mammalian cells remain under debate. Some mammalian cells can uptake and metabolize metal oxides nanoparticles[10, 11], but other findings emphasize risks for human and mammalian cells.[12, 13] Understanding the physicochemical behavior of nanostructured metal oxides in biological media and fluids is therefore essential for their applications in medicine.

Physicochemical properties that govern reactivity of nanostructured metal oxides are determined by particles size, shape, crystal structure and crystallographic orientation of

exposed facets – parameters which are mainly under the scope of surface science investigations. These studies are, however, restricted to the systematic use of single crystalline samples and to experiments in ultra-high vacuum i.e. to conditions that are far from physiological. However, it is well known that when exposing metal oxide nanostructures to water their surfaces undergo a series of chemical reactions which in turn, modify nanoparticles morphology, their dissolution properties or lead to the formation of new crystallographic phases. For instance, the most stable surfaces of MgO are by far those of (100) orientations leading to cubic crystallites with (100) facets. However, octahedra with (111) facets were found upon MgO dissolution in ultrapure water.[14, 15] Shape transformation was also observed for TiO_2 nanoparticles, where an excess dilution with deionized water caused partial dissolution of the cubic-like TiO_2 nanocrystals and, consequently, its transformation into spherical ones.[16] The solubility of nanoparticles was found to depend not only on their chemical properties but also on the particles size, shape, surface properties and crystal structure.[17] In contact with water a thermodynamically stable hydroxide layer is formed on the ZnO surface preventing further penetration of water into the bulk.[18] However, in nanostructured form, ZnO possesses a greater propensity for dissolution in water.[19]

In biological environments, the presence of plasma proteins, salt composition and pH value affect additionally morphology, surface chemistry, dissolution and aggregation degree of nanoparticles. When suspended in biological fluids nanoparticles rapidly associate with a series of proteins that form a dynamical layer all over the particle.[20] The formation of this so-called “protein-corona” layer modifies the original physicochemical properties of nanoparticles and determines their biocompatibility. The presence of serum proteins was shown to modify aggregation properties of different nanoparticles and consequently alters

their reactivity.[20, 21, 22, 23, 24] Initially nanoparticles are coated by the most abundant proteins as albumin, immunoglobulins and fibrinogen. These can be displaced over time by less abundant but higher affinity proteins in processes that are also in a function of the nanoparticles sizes and surface properties.[25, 26, 27] Finally, proteins bound to nanoparticles may undergo conformational and functional changes which in turn may alter their own reactivity.[26, 28, 29]

Recently, we have shown that ZnMgO nanoparticles exhibit an efficient antibacterial activity while being safe for human HeLa cells.[8] In this work, alternations in shape, surface structure and optical activity of ZnMgO nanoparticles were studied upon dissolution in water and some commonly used cell culture media. Attention was paid to the interaction between ZnMgO nanoparticles and serum proteins, in particular serum albumin (BSA). Those interactions were correlated with the nanoparticles toxicity towards mammalian cells.

Experimental section

Synthesis of ZnMgO nanoparticles

ZnMgO nanoparticles were fabricated by burning 10 wt % Mg/Zn alloy (Mg90/Zn10, 10 wt %, Goodfellow) in a glove box made of stainless steel and rigid plastic designed to afford vacuum (P ~ 1 mbar). The combustion of alloy ribbons was started by a thin Ni–Cr wire held in contact with the extremity of the ribbon which could be resistively heated. Prior to the measurements powders were kept and transported under vacuum ($p< 10^{-5}$ mbar) in order to prevent any contact with the ambient air.

Chemicals and proteins

NaCl (99.9 % purity), HEPES, Luria Bertani Broth (LB) medium, Crystal Violet and bovine serum albumin (BSA) were purchased from Sigma-Aldrich. Fetal bovine serum (FBS) was purchased from Perbio. Before use, Crystal Violet was dissolved in milliQ water (0.05 % w/v) and filtered at 0.22 nm. BSA was additionally purified using size-exclusion chromatography and a Superdex S200 column with an enhanced separation for molecular weights in the range 15 to 100 KDa. After purification, the BSA monomer concentration was determined using the extinction coefficient deduced from the protein composition of ε= 43,824 $M^{-1}.cm^{-1}$.

Transmission electron microscopy (TEM)

Transmission electron microscopy (TEM) measurements were achieved by using LaB6 JEOL JEM 2100 (JEOL, Japan) field emission transmission electron microscope operated at 200 kV and with 0.18 nm resolution. For cryo-TEM analysis, the microscope was equipped with a cryo pole piece and a drop of solution was deposited on a Quantifoil grid (MicroTools GmbH, Germany). The excess of solution was then blotted out with a filter paper, and before evaporation the grid was quench-frozen in liquid ethane to form a thin vitreous ice film. The grid was then maintained all the time at 90 K to prevent evaporation and crystallization of the ice film. The images were taken on an ultrascan 2k CCD camera (GATAN, USA) and with a JEOL low dose system (Minimum Dose System, MDS) to protect the thin ice film from any irradiation before imaging and to reduce irradiation during the image capture.

UV/ Vis spectroscopy

UV/ Vis absorption spectra of liquid and solid nanoparticles samples were collected on UV-Vis-NIR Varian Cary 5000 spectrophotometer. Diffuse reflectance mode and an integrating sphere were used for measurements on powders whereas, the Kubelka-Munk model was applied to derive the absorbance values from the respective reflectance values.

Tryptophan fluorescence measurements

Fluorescence measurements were performed with a FP-6200 spectrofluorimeter (JASCO, Tokyo, Japon) connected with a thermostatted cell holder at 20 °C, using a 1-cm path length quartz cell. BSA (6 µM) was incubated with ZnMgO nanoparticles (ranging from 0.01 to 0.5 mg/ml) in HBS buffer (10 mM HEPES, 150 mM NaCl, pH 7.4) for 2 hrs before measurements. The fluorescent spectra were acquired in the range of 290 to 450 nm when excited at 280 nm, at a scanning rate 125 nm/min, and a bandwidth 5 nm.

Circular dichroism (CD)

Far-UV (180-260 nm) CD spectra were measured on a JASCO J-810 spectropolarimeter using a 1 mm path length quartz cell. BSA (6 µM) was incubated with 0.1-1 mg/ml of ZnMgO in HBS buffer, pH 7.4, for 24 hrs before recording. Spectra were collected at a scanning rate of 100 nm/min, with a band width of 1.0 nm and a resolution of 100 mdeg. Measurements were done at 20°. Each spectrum was an average of 8 scans. All spectra were corrected for the contribution of the buffer.

Dynamic Light Scattering

Dynamic Light Scattering (DLS) measurements were performed on a Zetasizer Nano serie (Malvern, UK) using a helium-neon laser wavelength of 633 nm and detection angle of 173°. The scattering intensity data were processed using the instrumental software to obtain the hydrodynamic diameter (R_H) and the size distribution of particles in each sample. R_H of the particles was estimated from the autocorrelation function, using the Cumulants method. A total of 10 scans with an overall duration of 5 min were obtained for each sample. All measurements were done in HBS buffer, pH 7.4, at 20 °C.

Cell cultures and cytotoxicity tests

Madin-Darby canine kidney (MDCK) cells were used to test ZnMgO cytotoxicity. Cells were purchased from the American Type Culture Collection (Manassas, VA) and grown in MEM medium (minimum essential medium) supplemented with Earle's Salts without L-glutamine (PPA The Cell Culture Company, Austria), completed with 10% heat-inactivated FBS, 2 mM L-glutamine, penicillin (100 units/mL) and streptomycin (0.1 mg/mL), according to the American Type Culture Collection recommendations. Cells were maintained at 37°C in a 5 % CO_2 incubator. In some tests, cells were washed with FBS-free medium before incubation with nanoparticles.

Cell death was quantified by acridine orange staining followed by flow cytometry analysis (Becton FACSCalibur, Dickinson and Company, USA), as explained elsewhere.[8] Briefly, the cells were collected, washed in PBS (8 mM Na_2HPO_4, 1.5 mM KH_2PO_4, 150 mM NaCl, 3 mM KCl, pH 7.4), and then resuspended in the cellular medium containing acridine orange (0.1 µg/mL) in the dark. Stained cells were fixed with 3.2 % paraformaldehyde in PBS and

then collected and resuspended in PBS. Each test was done on $5x10^4$ cells.

A cytotoxicity test with the crystal violet staining was done on MDCK cells incubated with ZnMgO nanoparticles overnight. MDCK cellular monolayers were then fixed with 10 % formol and subsequently stained with crystal violet for 30 minutes.

Particles incubation with cell culture medium and SDS-PAGE analysis

ZnMgO (1 mg) was incubated with RPMI medium complemented with 10 % FBS overnight (total volume, 1ml). The particle-protein complexes were purified as previously explained.[27, 28] Briefly, samples were centrifuged at 14,000xg to pallet particle-protein complexes. The pallets were extensively washed in PBS buffer to remove all non-bound proteins. In the final step pallets were resuspended in the Laemmli buffer and boiled for 5 min at 100°C to eluted bound proteins from the particles. NuPage BisTris 12 % polyacrylamide gels (Invitrogen, France) were used for SDS-PAGE. All experiments were produced at least twice to ensure reproducibility of the particle-protein complex.

Results and Discussion

ZnMgO in water: morphology and optical properties

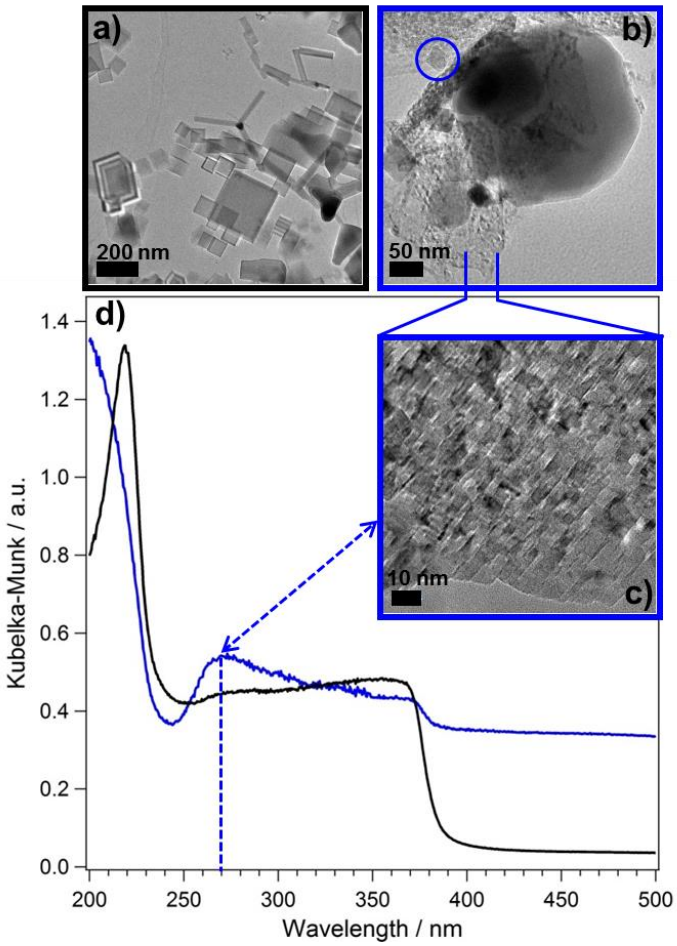

Figure 1: TEM images (a, b and c) and Diffuse Reflectance UV/Vis spectra (d) of as-synthetized ZnMgO nanopowders (black border and black curve) and water-treated (blue borders and blue curve). Powders were annealed (T=1270K, $p < 10^{-5}$mbar) and kept in vacuum ($p < 10^{-5}$ mbar) prior to measurements. The blue circle in (b) surrounds crystallites of octahedral form to point out non observable structures in as-synthetized powders. A region with disordered and fragmented structures in (b) was recorded at higher magnification and presented in (c) in the close-up view. The blue arrow correlates morphological modifications (fragmented structures) with corresponding optical feature in Diffuse Reflectance UV/Vis spectrum.

Prior to the study of ZnMgO under physiological conditions, the water effects on ZnMgO morphology and optical properties were investigated since water represents the major constituent in biological fluids and media. For this purpose, ZnMgO nanoparticles were treated with deionized water for 24h and subsequently annealed at 1270 K under high vacuum conditions. This thermal treatment provides completely dehydroxilated and adsorbate free surface of nanoparticles and represents an essential precondition in surface science investigation of highly dispersed metal oxides.[30] TEM images of as-synthesized and water-treated ZnMgO nanopowders are compared in Figure 1. As recently reported[8], as-synthesized ZnMgO exhibits shapes that are characteristic of both of its pure components, MgO-cubes and ZnO- tetrapods and rods (Figure 1a). In the same work, X-ray diffraction measurements were also conducted on the as-synthesized ZnMgO powder showing the coexistence of both crystal phases, cubic- and hexagonal. Thus, it was confirmed that ZnMgO powder represents a two-component system. Such ZnMgO morphology is characteristic for the synthesis route applied. , which moreover provides particles with low degree of aggregation[31] due to the particles generation in the gas-phase in combination with the above described annealing treatment Upon water treatment most MgO cubes undergo corrosion, preferentially at corner and edge sites, which results in the loss of their regular cubic shape and the appearance of octahedral shape, as designated by blue circle in Figure 1b. The observed cubic to octahedral transformation of MgO shape fully agrees with both, theoretical calculations[14, 32, 33] and experimental evidences reported previously.[15] It was shown that when immersed in water, MgO cubic crystallites limited by (100) facets firstly reveal average (110) cuts of the edges. These are followed by (111) cuts giving the crystallites an octahedral form. As for ZnO-part, the tetrapod- and nanorod-like shapes, which are characteristic for as-synthetized ZnMgO nanopowders (Figure 1a), could not be

any longer detected after the powder was treated with water (Figure 1b). This implies that ZnO nanoparticles partially dissolve in water. In addition, the pH value of ZnMgO water solution was measured to be ~ 9 indicating the formation OH^- ions. As a matter of fact, ZnO is one of the metal oxides most soluble in water and its major cytotoxicological impact is usually correlated with the released Zn^{2+} ions in a given biological environment.[34, 35, 36] Finally, disordered and fragmented structures were also detected in water treated ZnMgO, as presented in a close-up view in Figure 1c. Interestingly, such structures were not reported for water treated pure MgO[15] nor pure ZnO.[6]

Morphological changes of nanostructured materials result in the redistribution of specific surface sites and, therefore, can be easily tracked in their optical properties.[37] Diffuse Reflectance UV/Vis spectra obtained on as-synthesized and on water-treated ZnMgO powders are compared in Figure 1d. As expected, the spectrum of as-synthesized ZnMgO nanopowder represents a superimposition of spectra characteristic of pure oxides: two absorption bands, at 222 nm (band I) and 270 nm (band II) that correspond to MgO nanopowders and the absorption edge at about 375 nm which refers to ZnO. The absorption bands I and II were previously attributed to localized electronic transitions occurring at 4-fold and 3-fold coordinated oxygen anions in edges and corners of MgO cubes, respectively.[37, 38] In as-synthetized ZnMgO powder, the absorption band I shows a relatively high intensity while the absorption band II can only be noticed as an inflection (black curve in Figure 1d). Upon water treatment, an intensity enhancement was measured for the absorption band I. Additionally, it became broader with the maximum shifted below the wavelength accessible in non-evacuated spectrometers (λ>200 nm), enabling its complete characterization (blue curve in Figure 1d). However, the observed broadening of the band I suggests that some of MgO edges were affected by water. The water treatment significantly

increased the intensity of the absorption band II. Detection of this absorption band was shown to be possible only on MgO nanopowders with high concentration of 3-coordinated oxygen ions in corner position of MgO cubes.[37] Therefore, the intensity increase of band II indicates that the erosion of MgO nanocrystals upon water treatment results in formation of corner sites. This finding is consistent with the TEM observation of disordered/fragmented structures in Figure 1c. The blue arrow in Figure 1 associates the morphological modification with its corresponding reflection in the optical spectrum. Although ZnO specific nanorods and tertrapods were not microscopically detected in the water treated ZnMgO, the absorption edge characteristic of pure ZnO (~ 375 nm) was measured as slightly red shifted (Figure 1d, blue curve). Unlike MgO where electronic transitions are precisely assigned to certain surface sites, optical transitions in ZnO are delocalized within the whole bulk. The absorption intensity was seen to increase in $\lambda > 375$ nm, suggesting that new gap states in ZnO bulk were formed upon water treatment. Interestingly, such enhancement of absorption intensity was not observed for pure ZnO treated with water (Figure S-1, Supporting Information). The results demonstrate that both, the ZnO-specific and the MgO-specific spectroscopic characteristics of nanostructured ZnMgO are affected by water. This supports the microscopic evidence of morphological alternations observed in water treated ZnMgO samples.

ZnMgO behavior in biological media

The behavior of the ZnMgO nanopowder in two biological environments, LB bacteria growth and RPMI mammalian cell culture media was investigated by Cryo-TEM visualization and UV/Vis spectroscopy. The measurements were done directly in the solution in order to approach physiological conditions. Cryo-TEM images in Figure 2a (upper panel) reveal that

the morphology of ZnMgO suspended in LB bacterial medium for 24 hours was altered in a similar way as after water treatment. Indeed, most of MgO crystallites, which initially exhibit an exceptionally regular cubic shape, were transformed into octahedral forms; whereas ZnO nanorods and nanotetrapods, initially present in ZnMgO smoke powders, were not evidenced. However, unlike water treated samples, ZnMgO did not show disordered and fragmented structures in the LB medium. Admixing ZnMgO into the LB medium did not change its physiological pH (pH = 7.4). A recent dissolution kinetics study of nano-ZnO has shown that Zn^{2+} ions are hardly released from the oxide at neutral pH.[36] Thus, different pHs in water and the LB medium may contribute to diverse structural modifications observed for ZnMgO nano-crystals in two environments.

The UV/Vis absorption spectrum of ZnMgO dissolved in LB medium (Figure 2a) shows no optical features specific of ZnMgO nanopowder (Figure 1d). The main contribution to optical absorption of ZnMgO-LB solution originates from molecules present in the LB medium (Figure S-2a, Supplementary Information). LB contains many amino acids, especially tryptophan, NaCl (5 g/L) and yeast extract. An intensity loss was observed in the spectrum recorded after 24h compared to spectrum recorded immediately upon adding nanoparticles (Figure 2a). Similarly, an intensity decrease was found in UV/Vis spectra of pure components, MgO and ZnO (Figure S-3a). This intensity loss indicates that the concentration of molecules from medium decreases which may be explained by their binding to nanoparticles. The adsorption of these molecules will affect the reactivity of nanoparticles, since further interactions of nanoparticles will be mediated by the layer formed on their contact surface. Indeed, it was previously reported that the minimal antibacterial inhibitory concentration of nano-ZnO was around two orders of magnitude smaller in pure water than in the bacteria growth medium.[39] The authors proposed that molecules from the medium may compete

with the bacterial membrane to bind the nanoparticle which, in consequence, decreases the antibacterial efficiency of nano-ZnO.

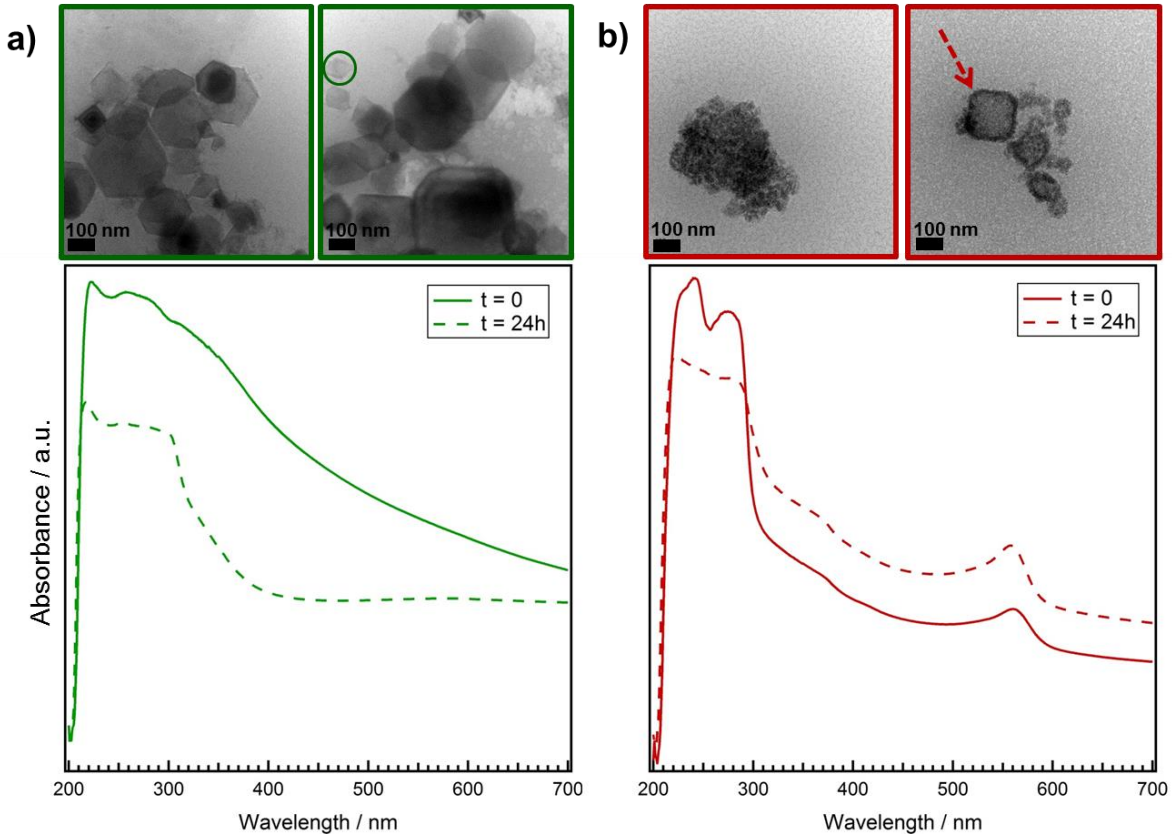

Figure 2: Cryo-TEM images and UV/Vis spectra of ZnMgO nanopowder admixed into (a) a LB bacterial medium (green) and (b) a RPMI mammalian cell culture medium supplemented with 10 % FBS (red). Nanoparticles were incubated for 24 hours within each medium before electron microscopy observations. The green circle indicates cubic to octahedral shape transformation occurred in LB medium. The red arrow indicates a form close to cubic. UV-Vis spectra were recorded immediately (solid lines) and after 24 hours (dashed lines) that ZnMgO was suspended.

After being dissolved in the mammalian cell culture RPMI medium complemented with 10 % fetal bovine serum (FBS), ZnMgO nanoparticles exhibited disordered and agglomerated structures (Figure 2b, upper panel). ZnO specific nanotetrapods and nanorods disappeared also in this medium, while MgO nanocubes were seen to be strongly damaged and to expose particularly irregular surfaces. However, some forms close to cubic were still recognizable, as highlighted by the red arrow in Figure 2b. The pH value of RPMI medium after admixing ZnMgO remained physiological. This indicates that medium buffer capacity neutralized hydroxide ion release observed in pure water solution. We assume that alternations of nanoparticles morphology in the mammalian cell culture medium comprise: (i) crystal fragmentation upon contact with water, (ii) adsorption of molecules from the medium and (iii) an agglomeration of the formed entities. Agglomeration of nanoparticles due to the high ionic strength of the biological environment is one of the main effects that accompany interaction between nanoparticles and biological molecules.[23] Nanoparticles are reported to be rapidly coated by various biomolecules, especially proteins, when dissolved in biological fluids and media.[16, 40] Indeed, Cryo-TEM images in Figure 2b show shapeless structures which can be assumed to be serum proteins forming corona over ZnMgO.

Similarly to LB, also in this medium UV/Vis spectroscopy did not reveal optical transitions that are typical of a ZnMgO nanopowder (Figure 2b), but mainly due to molecules of which the medium consists (Figure S-2b, Supplementary Information). After 24 hrs incubation of ZnMgO in completed-RPMI medium, absorption intensities decreased for the part of the spectrum between 200-300 nm while a quite visible intensity enhancement was observed in the range of higher wavelengths (Figure 2b). This intensity increase indicates the occurrence of new electronic transitions, which strongly suggests the formation of

complexes between ZnMgO and molecules from the medium. Interestingly, such intensity increase was not observed in absorption spectra of pure MgO and ZnO (Figure S-3b).

To verify ZnMgO-protein complex formation, a SDS-PAGE analysis was applied on ZnMgO nanoparticles incubated with the RPMI medium supplemented with 10 % FBS. After 24 hours of incubation, the solution was centrifuged to collect protein/nanoparticle complexes and pallets were subjected to gel migration. The obtained protein profile in Figure 3a indicates that the most abundant serum proteins, especially BSA with a molecular weight of about 66 kDa, were adsorbed on ZnMgO nanopowders.

ZnMgO-BSA interaction

BSA is reported to be rapidly associated with a range of nanoparticles of various composition and size.[41, 42, 43] By far the most abundant protein in blood serum, albumin is also the most abundant protein in the FBS supplemented RPMI medium (0.4 mg/ml according to manufacturers' specification). The UV/Vis absorption spectrum of pure BSA and BSA incubated with ZnMgO nanoparticles for 24 hrs is presented in Figure 3b. Pure BSA gives two characteristic absorption peaks: an intense one between 190-210 nm which is due to the transition in polypeptide backbone structure and the less intensive one at 280 nm attributed to absorption of aromatic amino acids.[44] Admixing ZnMgO to BSA clearly decreased the intensity of the absorption band centered at ~200 nm while intensity enhancement was seen in the full range of λ> 260 nm. This latter absorption was observed in UV/Vis spectrum recorded on water dissolved ZnMgO (inset in Figure 3b) and thus can be assigned to absorption properties of ZnMgO nanoparticles in an aqueous solution. Significant differences between UV/Vis spectra of pure BSA and BSA-ZnMgO system, both quantitative and qualitative, support the finding that BSA binds to ZnMgO nanocrystals.

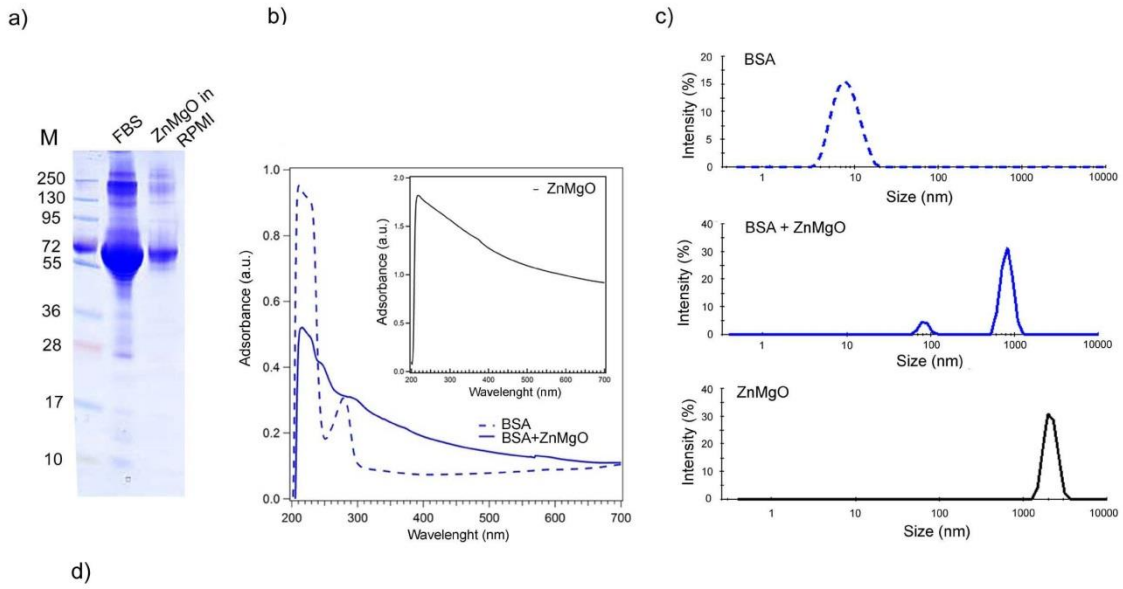

d)

Sample	Zeta-potential (mV)
BSA in HBS	-8 ± 1.9
ZnMgO in HBS	+3 ± 0.45
BSA+ZnMgO in HBS	-12 ± 0.3
ZnMgO in H_2O	+37 ± 2.2
ZnMgO in LB medium	-19 ± 1.4
ZnMgO in 10% FBS -RPMI medium	-13 ± 1.9

Figure 3. Interaction between ZnMgO nanoparticles and BSA. (a) Illustration of SDS-PAGE gel analysis of ZnMgO-associated proteins from RPMI medium supplemented with 10 % FBS. (b) UV/Vis spectra of pure BSA (0.4 mg/ml) dissolved in water and after admixing ZnMgO (1 mg/ml). Inset, UV/Vis spectrum of ZnMgO in water (1mg/ml). (c) Size distributions of monomeric BSA, BSA-ZnMgO mixture and pure ZnMgO nanoparticles in HBS buffer pH 7.4, monitored by DLS. All solutions were incubated for 24 hours at room temperature before measurements. (d) Zeta-potential of ZnMgO nanoparticles in different media used in this work.

Binding of BSA to ZnMgO was expected since one of the biological roles of this protein is to non-specifically bind and carry various molecules in blood. The interaction BSA-ZnMgO may be governed by electrostatic attractions between nanoparticles surface charges

and those of the protein amino acids. In addition, surrounding water molecules can facilitate these bindings as it was predicted from computer simulations of protein adsorption to MgO surface.[45] The interaction between nanoparticles, water and proteins from the medium may in turn influence the formation of agglomerates in solutions. Thus, DLS measurements were performed to find the mean hydrodynamic radius (R_H) of the BSA admixed to ZnMgO. As shown in Figure 3c the R_H of monomeric BSA in the buffer solution was about 8 nm which was expected for a globular protein of 66 kDa. Upon addition of ZnMgO, new peaks were observed designing species with apparent higher sizes of R_H = 85 nm and 820 nm (Figure 3c). Interestingly, ZnMgO nanoparticles alone gave large microscale clusters with R_H > 2100 nm. DLS data suggest that BSA stabilized dispersion of ZnMgO particles in the aqueous solution. Similar stabilizing effect of BSA on nanoparticle aggregation was previously reported for ZnO in water.[21]

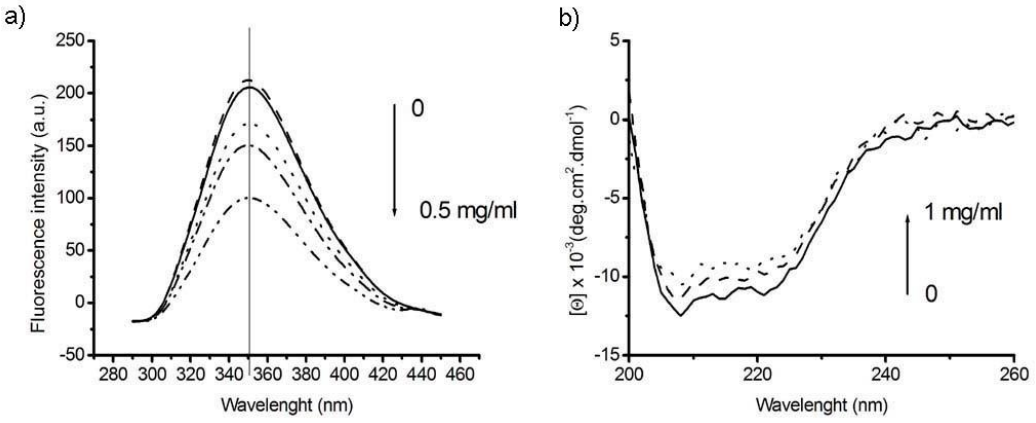

Figure 4. (a) Fluorescence spectra of BSA (0.4 mg/ml) alone and in the presence of different ZnMgO concentrations (0.01-0.5 mg/ml). Measurements were done in HBS buffer solution, pH 7.4. Note the decrease in protein fluorescence with increasing nanoparticle concentration. (b) Circular dichroism spectra of BSA in the absence (solide line) and in the presence of 0.1 mg/ml ZnMgO (3-point segment) and 1 mg/ml ZnMgO (2-point segment).

To verify whether BSA-ZnMgO interaction can be governed by electrostatic interaction zeta-potential measurements were performed in HBS buffer. The zeta potential is a key indicator of the stability of colloidal dispersions and represents the overall charge a particle acquires in a solution. As shown in Figure 3d, BSA had a negative surface charge while ZnMgO had a positive one. ZnMgO-BSA complex had a negative surface charge of higher magnitude of zeta-potential when compared to those obtained on two systems separately (Figure 3d). This suggests the formation of BSA-ZnMgO complex and confirms the proposed implication of electrostatic interactions in their binding. For comparison, zeta potential of ZnMgO was determined in water, LB and RMPI media (Figure 3d). Relatively high values of zeta potential were measured for ZnMgO in water and LB medium (37 mV and -19 mV, respectively) indicating that nanoparticles resist aggregation in these solutions as observed in TEM images in Figures 1b, c and 2a. In contrast, zeta potential of ZnMgO dissolved in RPMI supplemented with serum proteins was relatively small (-13 mV). This indicates that nanoparticles tend to coagulate or flocculate in completed RPMI medium which is in agreement with our microscopic measurements in Figure 2b.

Certain proteins change their conformation and denature after being adsorbed on nanoparticles.[26, 28, 46] By fluorescence spectroscopy, we investigated whether the conformation of BSA is modified upon its adsorption on ZnMgO. Figure 4a shows the fluorescent emission spectra of BSA alone and when incubated with ZnMgO in concentration range from 0 to 0.5 mg/ml. The main contribution to the fluorescence of BSA is by tryptophan (Trp) which is very sensitive to the polarity of its environment.[47] In hydrophilic solutions, as when Trp is in contact with surrounding water molecules, its emission maximum is at about 355 nm. In a hydrophobic environment, as happened when Trp is not flexible but within the polypeptide ordered secondary structures, this maximum is blue

shifted.[47] As shown in Figure 4a upon admixing ZnMgO to the BSA solution, the maximum of Trp fluorescence did not shift but the intensity of the emission gradually decreased. The observed fluorescence quenching can result from the protein secondary structure rearrangement or by the formation of a nonfluorescent ground state complex between Trp and ZnMgO. To verify whether BSA undergoes secondary structure alternations upon binding to ZnMgO, CD spectra in far-UV region were recorded (Figure 4b). Two negative bands at 208 nm and 222 nm characteristic for α-helix structure of BSA are clearly visible in the spectra of BSA alone. Both of negative minimums decreased in intensity by adding 0.1 mg/ml and 1 mg/ml of nano-ZnMgO, whereas the peaks shape and position were almost unaffected. This implies that upon binding to ZnMgO, BSA preserves its initial structure but the protein α-helical content slightly decreases. A constant position of the Trp fluorescent maximum and a relatively small CD spectra alternation in Figure 4, suggest that the interactions between ZnMgO nanoparticles and BSA are weak.

ZnMgO toxicity towards mammalian cells

Finally, the toxicity of ZnMgO nanoparticles towards mammalian cells was investigated in a function of surrounding medium. The MDCK cells were incubated for 24 hours with ZnMgO nanoparticles (0.1 mg/ml and 1 mg/ml concentrations) in a medium containing various concentrations of serum proteins. MDCK cells were chosen for their robust growth in a serum-free medium. After incubation with nanoparticles, MDCK cell monolayers were stained with crystal violet to visualize the cytotoxic effect (Figure 5a). ZnMgO at 0.1 mg/ml showed no toxicity regardless of the serum protein concentration in the medium. However, a complete cell death was observed for 1 mg/ml of ZnMgO nanoparticles in FBS-free medium (Figure 5a). The cytotoxicity of ZnMgO was further

evaluated using acridine orange fluorescent staining to quantify damaged cells. MDCK cells incubated with ZnMgO were stained with acridine orange and the fluorescence was measured in a flow cytometer (Figure 5b). The acridine orange derived fluorescence intensity of untreated MDCK cells and cells treated with 0.1 mg/ml ZnMgO was unaffected regardless of the medium composition. In contrast, at 1 mg/ml and in the absence of FBS, ZnMgO nanoparticles killed about 85 % of the treated MDCK cells. These findings strongly suggest that serum proteins have a protective role against ZnMgO nanoparticle toxicity. Interestingly, 1% FBS was sufficient to fully protect MDCK cell from ZnMgO toxicity (Figure 5). Probably, even at low serum concentration the ZnMgO surface is fully covered by serum proteins. Similar effect was previously observed during the formation of protein corona on nanoparticles at different plasma concentrations.[48]

Since albumin was detected as a major component in ZnMgO protein corona, we also tested the role of albumin in preventing cytotoxicity. For this purpose, we replaced serum by pure BSA at 0.4 mg/ml (equivalent BSA concentration in the medium). When MDCK cells grown in BSA complemented medium were incubated with ZnMgO nanoparticles less than 7 % cells survived, compared to 98% in medium containing FBS (Figure S-4, Supplementary Information). This suggests only a weak BSA protecting effect and indicates that BSA alone cannot prevent ZnMgO cytotoxicity. Probably other, less abundant serum proteins exert the protective role against ZnMgO cytotoxicity. Likewise, the dynamic formation of protein corona was shown to be a collective process that resulted in a creation of a stable heterogeneous layer at the nanoparticles surface.[48] Additional studies are, however, necessary to characterize other serum proteins binding to ZnMgO nanoparticles.

We previously have shown that 1 mg/ml ZnMgO was safe for human HeLa cells in a cellular medium containing 10 % FBS.[8] This is in accordance with the ZnMgO biocompatibility

observed here for MDCK cells in serum-containing medium. However, in bacterial growth LB medium 1 mg/ml of ZnMgO completely irradiated Gram-positive but not Gram-negative bacteria.[8] It appears, thus, that ZnMgO cellular toxicity depends on the cell–type and can be modulated by the composition of the surrounding medium.

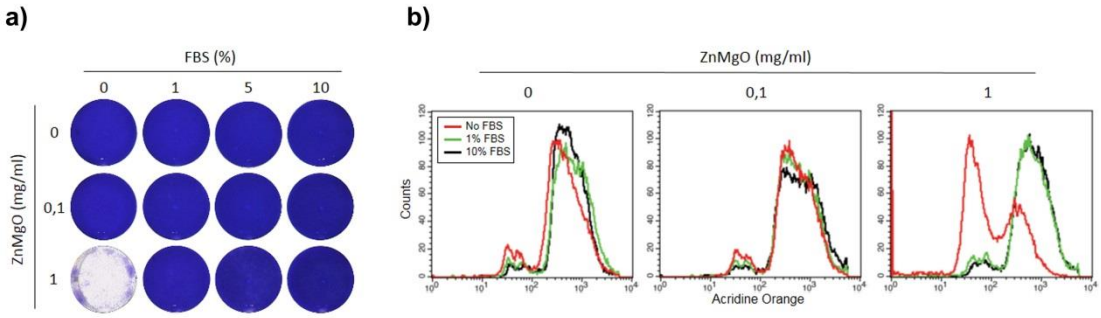

Figure 5. ZnMgO effects on cell viability. MDCK cells were incubated with ZnMgO nanopowders in a cell culture medium containing various concentrations of serum proteins for 24 hours. (a) MDCK cell monolayers were then stained with crystal violet, or (b) subjected to the flow cytometry analysis after acridine orange staining. Note that cell death was detected only in FSB-free medium for high nanoparticles concentration (1 mg/ml).

Conclusions

ZnMgO nanoparticles were observed to undergo morphological changes when admixed to aqueous solutions. In a complex cell culture medium the majority of nanoparticles become shapeless, agglomerated and coated with surrounding proteins. Consequently, mammalian cells encounter morphologically modified ZnMgO nanoparticles whose contact surfaces are

altered by the proteins in the corona. We conclude that the corona governs the cytotoxicity of the nanoparticles since the cellular damages caused by ZnMgO may be obstructed by proteins from surrounding media. We envisage that our overall results may shed light on the factors to be considered before applying metal oxide nanoparticles as new therapeutics.

Acknowledgement

We thank Charles-Adrien Richard (INRA, Jouy en Josas) for his help with size-exchange chromatography, David Portehault (LCMCP, Paris) for helping with zeta-potential measurements and Prof. Philippe Depondt (INSP, UPMC, Paris) for comments and proofreading.

For TOC only

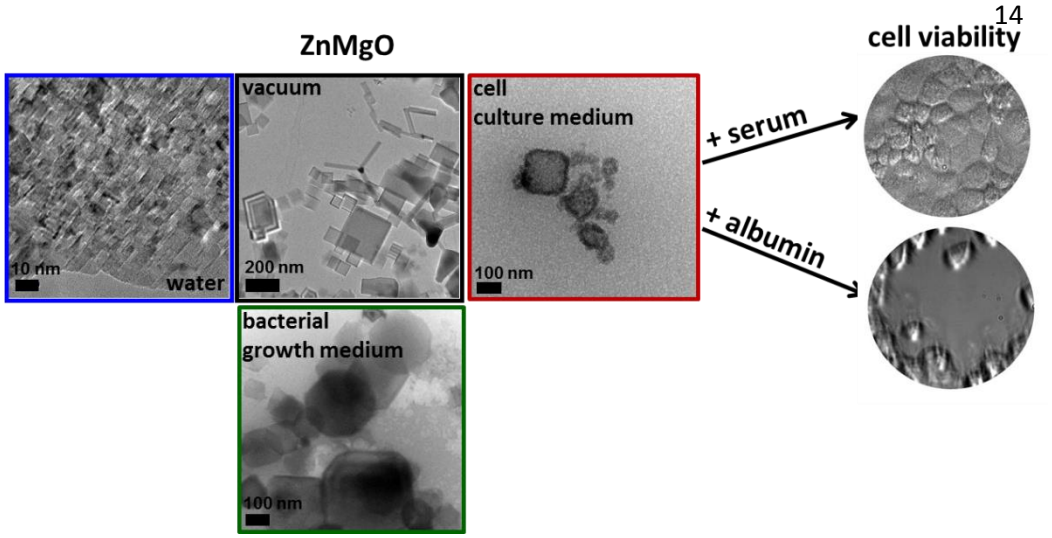

References

1. Henrich, V. E.; Cox, P. A. *The Surface Chemistry of Metal Oxides*; Cambridge University Press: Cambridge, UK, 1994.
2. Rodríguez, J. A.; Fernández-García, M. E. *Synthesis, Properties and Applications of Oxide Nanoparticles.*; Whiley: New Jersey2007.
3. Chertok, B.; Moffat, B. A.; David, A. E.; Yu, F.; Bergemann, C.; Ross, B. D.; Yang, V. C. Iron oxide nanoparticles as a drug delivery vehicle for MRI monitored magnetic targeting of brain tumors. *Biomaterials* 2008, *29* (4), 487-96.
4. Kievit, F. M.; Zhang, M. Surface engineering of iron oxide nanoparticles for targeted cancer therapy. *Acc Chem Res* 2011, *44* (10), 853-62.
5. Tassa, C.; Shaw, S. Y.; Weissleder, R. Dextran-coated iron oxide nanoparticles: a versatile platform for targeted molecular imaging, molecular diagnostics, and therapy. *Acc Chem Res* 2011, *44* (10), 842-52.
6. Brayner, R.; Dahoumane, S. A.; Yepremian, C.; Djediat, C.; Meyer, M.; Coute, A.; Fievet, F. ZnO nanoparticles: synthesis, characterization, and ecotoxicological studies. *Langmuir* 2010, *26* (9), 6522-8.
7. Hajipour, M. J.; Fromm, K. M.; Ashkarran, A. A.; Jimenez de Aberasturi, D.; de Larramendi, I. R.; Rojo, T.; Serpooshan, V.; Parak, W. J.; Mahmoudi, M. Antibacterial properties of nanoparticles. *Trends Biotechnol* 2012, *30* (10), 499-511.
8. Vidic, J.; Stankic, S.; Haque, F.; Ciric, D.; Le Goffic, R.; Vidy, A.; Jupille, J.; Delmas, B. Selective antibacterial effects of mixed ZnMgO nanoparticles. *J Nanopart Res* 2013, *15* (5), 1595.
9. Applerot, G.; Lellouche, J.; Lipovsky, A.; Nitzan, Y.; Lubart, R.; Gedanken, A.; Banin, E. Understanding the antibacterial mechanism of CuO nanoparticles: revealing the route of induced oxidative stress. *Small* 2012, *8* (21), 3326-37.
10. Arbab, A. S.; Wilson, L. B.; Ashari, P.; Jordan, E. K.; Lewis, B. K.; Frank, J. A. A model of lysosomal metabolism of dextran coated superparamagnetic iron oxide (SPIO) nanoparticles: implications for cellular magnetic resonance imaging. *NMR Biomed* 2005, *18* (6), 383-9.
11. Taylor, E.; Webster, T. J. Reducing infections through nanotechnology and nanoparticles. *Int J Nanomedicine* 2011, *6*, 1463-73.
12. Shi, J.; Karlsson, H. L.; Johansson, K.; Gogvadze, V.; Xiao, L.; Li, J.; Burks, T.; Garcia-Bennett, A.; Uheida, A.; Muhammed, M.; Mathur, S.; Morgenstern, R.; Kagan, V. E.; Fadeel, B. Microsomal glutathione transferase 1 protects against toxicity induced by silica nanoparticles but not by zinc oxide nanoparticles. *ACS Nano* 2012, *6* (3), 1925-38.
13. Turney, T. W.; Duriska, M. B.; Jayaratne, V.; Elbaz, A.; O'Keefe, S. J.; Hastings, A. S.; Piva, T. J.; Wright, P. F.; Feltis, B. N. Formation of zinc-containing nanoparticles from Zn(2)(+) ions in cell culture media: implications for the nanotoxicology of ZnO. *Chem Res Toxicol* 2012, *25* (10), 2057-66.
14. Geysermans, P.; Finocchi, F.; Goniakowski, J.; Hacquart, R.; Jupille, J. Combination of (100), (110) and (111) facets in MgO crystals shapes from dry to wet environment. *Phys Chem Chem Phys* 2009, *11* (13), 2228-33.
15. Hacquart, R.; Jupille, J. Hydrated MgO smoke crystals from cubes to octahedra. *Chemical Physics Letters* 2007, *439*, 91-94.
16. Gao, Y.; Elder, S. A. TEM study of TiO2 nanocrystals with different particle size and shape. *Materials Letters* 2000, *44*, 228–232.

17. Misra, S. K.; Dybowska, A.; Berhanu, D.; Luoma, S. N.; Valsami-Jones, E. The complexity of nanoparticle dissolution and its importance in nanotoxicological studies. *Sci Total Environ* 2012, *438*, 225-32.
18. Hu, X.; Masuda, Y.; Ohji, T.; Kato, K. Dissolution−Recrystallization Induced Hierarchical Structure in ZnO: Bunched Roselike and Core−Shell-like Particles. *Crystal Growth & Design* 2010, *10*, 626-631.
19. Bian, S. W.; Mudunkotuwa, I. A.; Rupasinghe, T.; Grassian, V. H. Aggregation and dissolution of 4 nm ZnO nanoparticles in aqueous environments: influence of pH, ionic strength, size, and adsorption of humic acid. *Langmuir* 2011, *27* (10), 6059-68.
20. Lynch, I.; Dawson, K. A. Protein-nanoparticle interactions. *Nanotoday* 2008, *3* (1-2), 40-47.
21. Churchman, A. H.; Wallace, R.; Milne, S. J.; Brown, A. P.; Brydson, R.; Beales, P. A. Serum albumin enhances the membrane activity of ZnO nanoparticles. *Chem Commun (Camb)* 2013, *49* (39), 4172-4.
22. Murdock, R. C.; Braydich-Stolle, L.; Schrand, A. M.; Schlager, J. J.; Hussain, S. M. Characterization of nanomaterial dispersion in solution prior to in vitro exposure using dynamic light scattering technique. *Toxicol Sci* 2008, *101* (2), 239-53.
23. Prasad, R. Y.; Wallace, K.; Daniel, K. M.; Tennant, A. H.; Zucker, R. M.; Strickland, J.; Dreher, K.; Kligerman, A. D.; Blackman, C. F.; Demarini, D. M. Effect of treatment media on the agglomeration of titanium dioxide nanoparticles: impact on genotoxicity, cellular interaction, and cell cycle. *ACS Nano* 2013, *7* (3), 1929-42.
24. Hsiao, I. L.; Huang, Y. J. Effects of serum on cytotoxicity of nano- and micro-sized ZnO particles. *J Nanopart Res* 2013, *15*, 1829.
25. Barran-Berdon, A. L.; Pozzi, D.; Caracciolo, G.; Capriotti, A. L.; Caruso, G.; Cavaliere, C.; Riccioli, A.; Palchetti, S.; Lagana, A. Time evolution of nanoparticle-protein corona in human plasma: relevance for targeted drug delivery. *Langmuir* 2013, *29* (21), 6485-94.
26. Cedervall, T.; Lynch, I.; Lindman, S.; Berggard, T.; Thulin, E.; Nilsson, H.; Dawson, K. A.; Linse, S. Understanding the nanoparticle-protein corona using methods to quantify exchange rates and affinities of proteins for nanoparticles. *Proc Natl Acad Sci U S A* 2007, *104* (7), 2050-5.
27. Lundqvist, M.; Stigler, J.; Elia, G.; Lynch, I.; Cedervall, T.; Dawson, K. A. Nanoparticle size and surface properties determine the protein corona with possible implications for biological impacts. *Proc Natl Acad Sci U S A* 2008, *105* (38), 14265-70.
28. Maiorano, G.; Sabella, S.; Sorce, B.; Brunetti, V.; Malvindi, M. A.; Cingolani, R.; Pompa, P. P. Effects of cell culture media on the dynamic formation of protein-nanoparticle complexes and influence on the cellular response. *ACS Nano* 2010, *4* (12), 7481-91.
29. Simon-Vazquez, R.; Lozano-Fernandez, T.; Peleteiro-Olmedo, M.; Gonzalez-Fernandez, A. Conformational changes in human plasma proteins induced by metal oxide nanoparticles. *Colloids Surf B Biointerfaces* 2014, *113*, 198-206.
30. Muller, M.; Stankic, S.; Diwald, O.; Knozinger, E.; Sushko, P. V.; Trevisanutto, P. E.; Shluger, A. L. Effect of protons on the optical properties of oxide nanostructures. *J Am Chem Soc* 2007, *129* (41), 12491-6.
31. Stankic, S.; Cotturac, M.; Demaillea, D.; Nogueraa, C.; Jupillea, J. Nucleation and growth concepts applied to the formation of a stoichiometric compound in a gas phase: The case of MgO smoke. *Journal of Crystal Growth* 2011, *329*, 52-56.
32. Pojani, A.; Finocchi, F.; Goniakowski, J.; Noguera, C. A theoretical study of the stability and electronic structure of the polar {111} face of MgO. *Surface Science* 1997, *387*, 354-370.
33. Refson, K.; Wogelius, R. A.; Fraser, D. G.; Payne, M. C.; Lee, M. H.; Milman, V. Water chemisorption and reconstruction of the MgO surface. *Physical Review B* 1997, *52*, 10823-10826.
34. Auffan, M.; Rose, J.; Wiesner, M. R.; Bottero, J. Y. Chemical stability of metallic nanoparticles: a parameter controlling their potential cellular toxicity in vitro. *Environ Pollut* 2009, *157* (4), 1127-33.
35. Zhang, H.; Ji, Z.; Xia, T.; Meng, H.; Low-Kam, C.; Liu, R.; Pokhrel, S.; Lin, S.; Wang, X.; Liao, Y. P.; Wang, M.; Li, L.; Rallo, R.; Damoiseaux, R.; Telesca, D.; Madler, L.; Cohen, Y.; Zink, J. I.; Nel, A. E.

Use of metal oxide nanoparticle band gap to develop a predictive paradigm for oxidative stress and acute pulmonary inflammation. *ACS Nano* 2012, *6* (5), 4349-68.

36. Chusueia, C. C.; Wub, C.-H.; Mallavarapua, S.; Houc, F. Y. S.; Hsud, C.-M.; Winiarze, J. G.; Aronstamb, R. S.; Huangb, Y.-W. Cytotoxicity in the age of nano: The role of fourth period transition metal oxide nanoparticle physicochemical properties. *Chemico-Biological Interactions* 2013, *206*, 319-326.

37. Stankic, S.; Muller, M.; Diwald, O.; Sterrer, M.; Knozinger, E.; Bernardi, J. Size-dependent optical properties of MgO nanocubes. *Angew Chem Int Ed Engl* 2005, *44* (31), 4917-20.

38. Hacquart, R.; Krafft, J.-M.; Costentin, G.; Jupille, J. Evidence for emission and transfer of energy from excited edge sites of MgO smokes by photoluminescence experiments. *Surface Science* 2005, *595*, 172–182.

39. Apperlot, G.; Lipovsky, A.; Dror, R.; Perkas, N.; Nitzan, Y.; Lubart, R.; Gedanken, A. Enhanced antibacterial activity of nanocrystalline ZnO due to increased ROS-mediated cell injury. *Adv Funct Mater* 2009, *19*, 842-852.

40. Yang, S. T.; Liu, Y.; Wang, Y. W.; Cao, A. Biosafety and bioapplication of nanomaterials by designing protein-nanoparticle interactions. *Small* 2013, *9* (9-10), 1635-53.

41. Allemann, E.; Gravel, P.; Leroux, J. C.; Balant, L.; Gurny, R. Kinetics of blood component adsorption on poly(D,L-lactic acid) nanoparticles: evidence of complement C3 component involvement. *J Biomed Mater Res* 1997, *37* (2), 229-34.

42. Lundqvist, M.; Stigler, J.; Cedervall, T.; Berggard, T.; Flanagan, M. B.; Lynch, I.; Elia, G.; Dawson, K. The evolution of the protein corona around nanoparticles: a test study. *ACS Nano* 2011, *5* (9), 7503-9.

43. Mahmoudi, M.; Lynch, I.; Ejtehadi, M. R.; Monopoli, M. P.; Bombelli, F. B.; Laurent, S. Protein-nanoparticle interactions: opportunities and challenges. *Chem Rev* 2011, *111* (9), 5610-37.

44. Layne, E. Spectrophotometric and Turbidimetric Methods for Measuring Proteins. . *Methods in Enzymology* 1957, *3*, 447-455.

45. Cormack, A. N.; Lewis, R. J.; Goldstein, A. H. Computer Simulation of Protein Adsorption to a Material Surface in Aqueous Solution: Biomaterials Modeling of a Ternary System. . *J. Phys. Chem.* 2004, *108*, 20408-20418.

46. Clift, M. J.; Bhattacharjee, S.; Brown, D. M.; Stone, V. The effects of serum on the toxicity of manufactured nanoparticles. *Toxicol Lett* 2010, *198* (3), 358-65.

47. Li, Q.; Chevalier, C.; Henry, C.; Richard, C. A.; Moudjou, M.; Vidic, J. Shadoo binds lipid membranes and undergoes aggregation and fibrillization. *Biochem Biophys Res Commun* 2013, *438* (3), 519-25.

48. Monopoli, M. P.; Walczyk, D.; Campbell, A.; Elia, G.; Lynch, I.; Bombelli, F. B.; Dawson, K. A. Physical-chemical aspects of protein corona: relevance to in vitro and in vivo biological impacts of nanoparticles. *J Am Chem Soc* 2011, *133* (8), 2525-34.

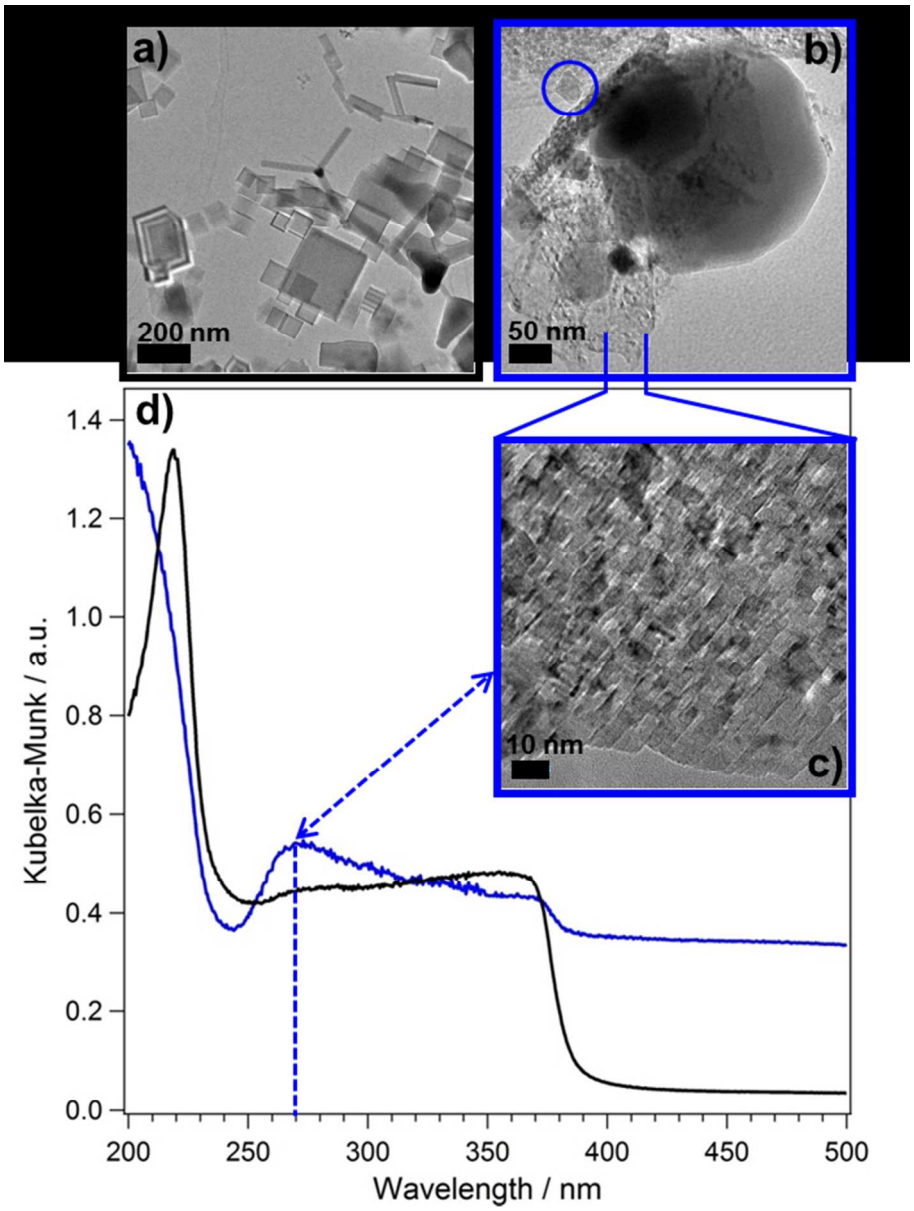

TEM images (a, b and c) and Diffuse Reflectance UV/Vis spectra (d) of as-synthetized ZnMgO nanopowders (black border and black curve) and water-treated (blue borders and blue curve). Powders were annealed (T=1270K, p < 10-5mbar) and kept in vacuum (p < 10-5 mbar) prior to measurements. The blue circle in (b) surrounds crystallites of octahedral form to point out non observable structures in as-synthetized powders. A region with disordered and fragmented structures in (b) was recorded at higher magnification and presented in (c) in the close-up view. The blue arrow correlates morphological modifications (fragmented structures) with corresponding optical feature in Diffuse Reflectance UV/Vis spectrum.
118x156mm (150 x 150 DPI)

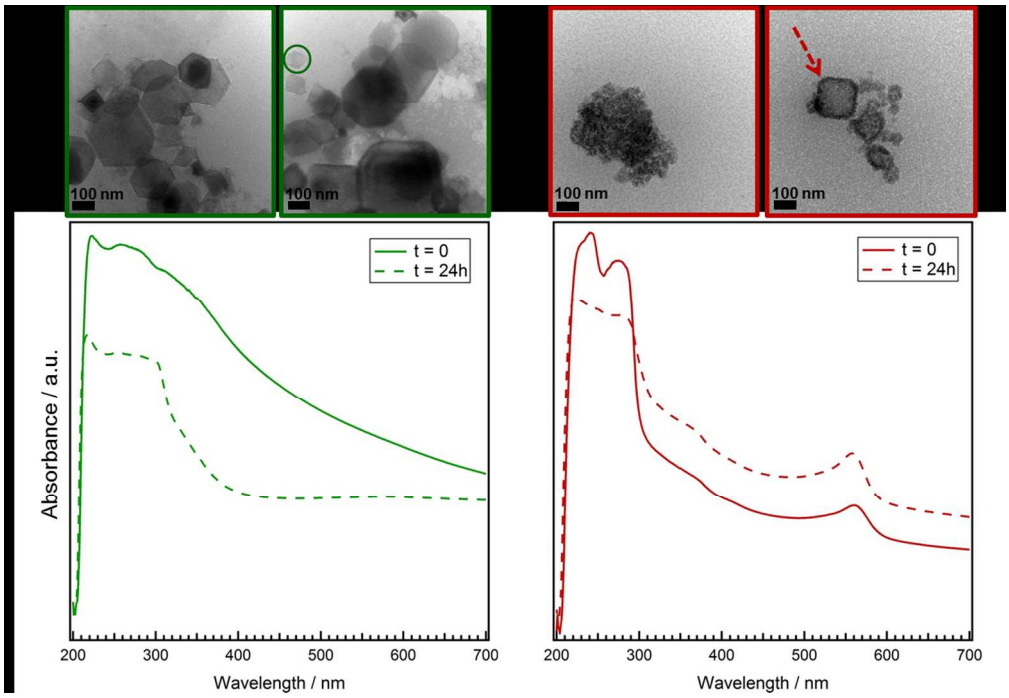

Cryo-TEM images and UV/ Vis spectra of ZnMgO nanopowder admixed into (a) a LB bacterial medium (green) and (b) a RPMI mammalian cell culture medium supplemented with 10 % FBS (red). Nanoparticles were incubated for 24 hours within each medium before electron microscopy observations. The green circle indicates cubic to octahedral shape transformation occurred in LB medium. The red arrow indicates a form close to cubic. UV-Vis spectra were recorded immediately (solid lines) and after 24 hours (dashed lines) that ZnMgO was suspended.
225x154mm (150 x 150 DPI)

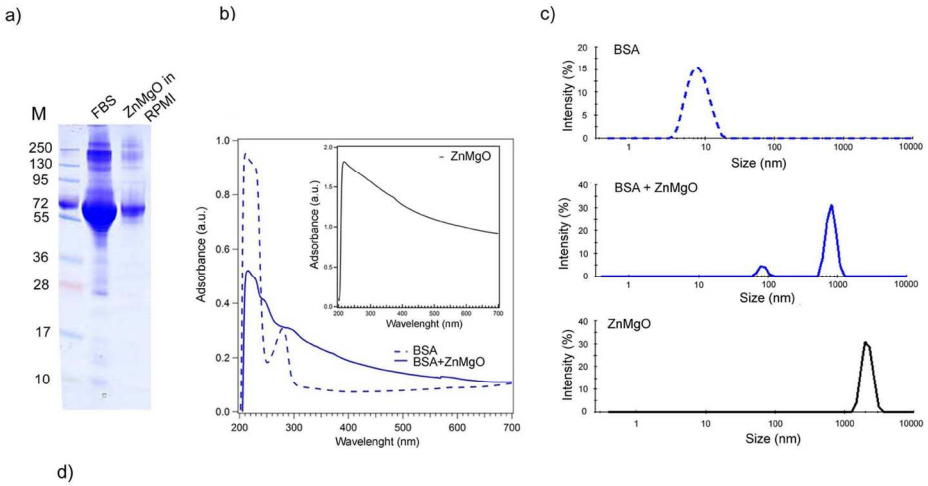

d)

Sample	Zeta-potential (mV)
BSA in HBS	-8 ± 1.9
ZnMgO in HBS	+3 ± 0.45
BSA+ZnMgO in HBS	-12 ± 0.3
ZnMgO in H_2O	+37 ± 2.2
ZnMgO in LB medium	-19 ± 1.4
ZnMgO in 10% FBS -RPMI medium	-13 ± 1.9

Interaction between ZnMgO nanoparticles and BSA. (a) Illustration of SDS-PAGE gel analysis of ZnMgO-associated proteins from RPMI medium supplemented with 10 % FBS. (b) UV/Vis spectra of pure BSA (0.4 mg/ml) dissolved in water and after admixing ZnMgO (1 mg/ml). Inset, UV/Vis spectrum of ZnMgO in water (1mg/ml). (c) Size distributions of monomeric BSA, BSA-ZnMgO mixture and pure ZnMgO nanoparticles in HBS buffer pH 7.4, monitored by DLS. All solutions were incubated for 24 hours at room temperature before measurements. (d) Zeta-potential of ZnMgO nanoparticles in different media used in this work.
124x91mm (300 x 300 DPI)

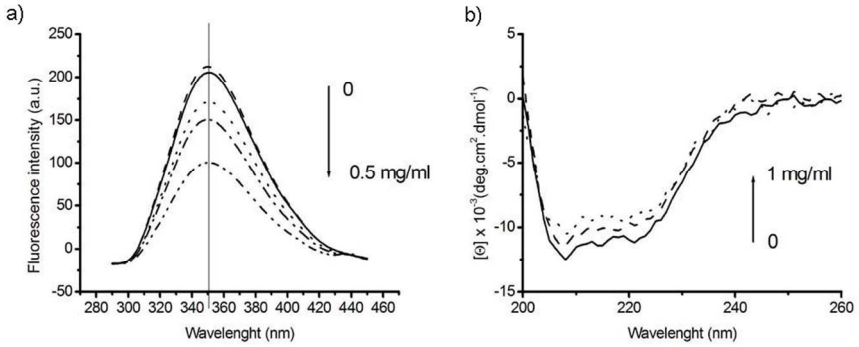

Fluorescence spectra of BSA (0.4 mg/ml) alone and in the presence of different ZnMgO concentrations (0.01-0.5 mg/ml). Measurements were done in HBS buffer solution, pH 7.4. Note the decrease in protein fluorescence with increasing nanoparticle concentration. (b) Circular dichroism spectra of BSA in the absence (solide line) and in the presence of 0.1 mg/ml ZnMgO (3-point segment) and 1 mg/ml ZnMgO (2-point segment).
199x71mm (150 x 150 DPI)

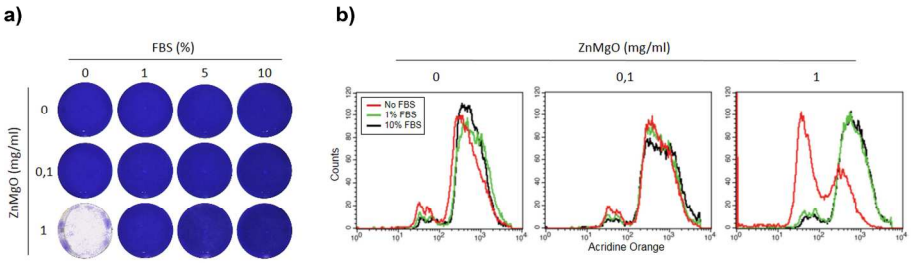

ZnMgO effects on cell viability. MDCK cells were incubated with ZnMgO nanopowders in a cell culture medium containing various concentrations of serum proteins for 24 hours. (a) MDCK cell monolayers were then stained with crystal violet, or (b) subjected to the flow cytometry analysis after acridine orange staining. Note that cell death was detected only in FSB-free medium for high nanoparticles concentration (1 mg/ml).

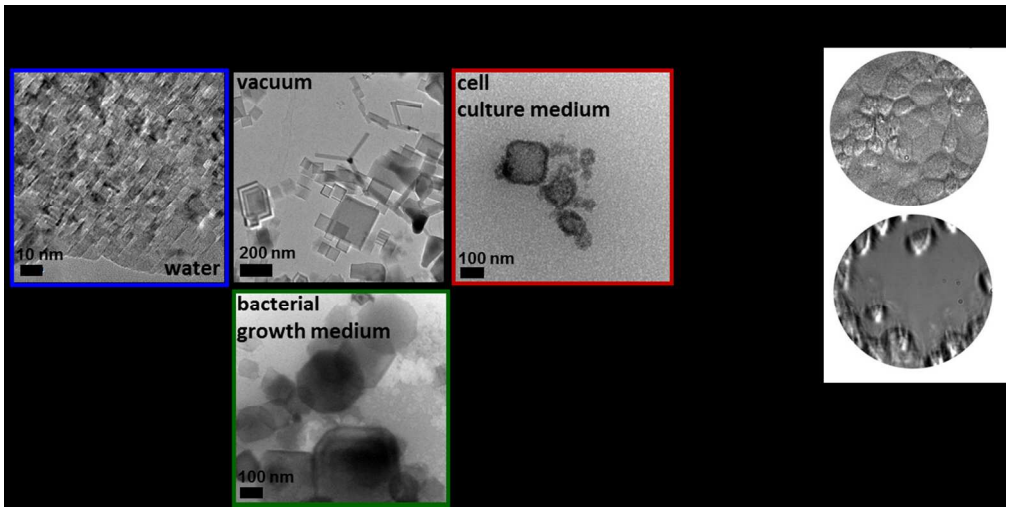

214x107mm (150 x 150 DPI)